ORIGINAL ARTICLE

GSDMD in peripheral myeloid cells regulates microglial immune training and neuroinflammation in Parkinson's disease

Bingwei Wang [a,*,†], Yan Ma [a,†], Sheng Li [b,†], Hang Yao [b], Mingna Gu [a], Ying Liu [a], You Xue [a], Jianhua Ding [b], Chunmei Ma [b,*], Shuo Yang [b,*], Gang Hu [a,b,*]

[a] School of Medicine & Holistic Integrative Medicine, Nanjing University of Chinese Medicine, Nanjing 210023, China
[b] School of Basic Medical Sciences, Nanjing Medical University, Nanjing 211166, China

Abstract Peripheral bacterial infections without impaired blood−brain barrier integrity have been attributed to the pathogenesis of Parkinson's disease (PD). Peripheral infection promotes innate immune training in microglia and exacerbates neuroinflammation. However, how changes in the peripheral environment mediate microglial training and exacerbation of infection-related PD is unknown. In this study, we demonstrate that GSDMD activation was enhanced in the spleen but not in the CNS of mice primed with low-dose LPS. GSDMD in peripheral myeloid cells promoted microglial immune training, thus exacerbating neuroinflammation and neurodegeneration during PD in an IL-1R-dependent manner. Furthermore, pharmacological inhibition of GSDMD alleviated the symptoms of PD in experimental PD models. Collectively, these findings demonstrate that GSDMD-induced pyroptosis in myeloid cells initiates neuroinflammation by regulating microglial training during infection-related PD. Based on these findings, GSDMD may serve as a therapeutic target for patients with PD.

*Corresponding authors.

E-mail addresses: ghu@njmu.edu.cn (Gang Hu), shuoyang@njmu.edu.cn (Shuo Yang), bingweiwang@njucm.edu.cn (Bingwei Wang), macm@njmu.edu.cn (Chunmei Ma).

†These authors made equal contributions to this work.

1. Introduction

As average life expectancy continues to grow, an increasing percentage of the population is developing a higher risk of developing neurodegenerative diseases, such as Alzheimer's disease and Parkinson's disease (PD). PD is characterized by a dramatic loss of dopaminergic neurons in the substantia nigra (SN), which leads to significant disability and a massive decrease in life expectancy and quality of life[1]. Although the pathogenesis of PD has not been fully elucidated, it is well known that peripheral infections can influence etiology and PD progression[2]. For instance, the carriers of the Gram-negative bacterium *Helicobacter pylori* experience a significant increase in morbidity of PD[3−5]. Periodontal infections can also increase the incidence of PD[6]. In addition to epidemiological factors, a recent study found that mice deficient for the PD-related gene, *Pink1*, develop a PD-like pathological phenotype in response to intestinal infection with Gram-negative bacteria[7]. Collectively, these studies indicate that PD progression can be greatly impacted by bacterial infections. The blood−brain barrier (BBB) confers a sterile state in the central nervous system (CNS) by preventing the infiltration of pathogens, toxins, and immune cells into parenchyma[8,9]. However, the underlying mechanism by which peripheral infection triggers PD beyond an intact BBB is not well defined.

Innate immune memory is an essential systematic reprogramming of innate immune cells, including macrophages, which occurs in response to stimuli and alters the subsequent scale of secondary immune responses[10,11]. Innate immune memory is divided into two forms: "immune training" and "immune tolerance", which refer to enhanced or suppressed immune responses upon secondary stimulation, respectively[11−13]. In the periphery, immune training has been shown to enhance pathogen clearance[14,15]. Innate immune training in monocytes also contributes to the pathogenesis of atherosclerosis[16]. Microglia, the resident macrophages of CNS, are "primed" by inflammatory stimuli and become sensitized to subsequent secondary inflammatory stimuli. Moreover, some studies have identified critical roles for microglial priming in CNS pathologies, such as prion disease, aging, experimental autoimmune encephalomyelitis, and Wallerian degeneration[17−20]. Intriguingly, a recent study showed that microglia could develop long-lasting immune memory following repeated exposures to systemic low-dose lipopolysaccharide (LPS) with an intact BBB. Brain-specific immune training was induced following a second exposure to LPS ($2 \times$ LPS), indicating that the level of pro-inflammatory cytokines is increased in the brain after the first exposure to LPS ($1 \times$ LPS). Strikingly, immune training in microglia triggered by peripheral inflammation exacerbates neuroinflammation in Alzheimer's disease[21]. However, the specific signals that confer trained status on microglia and how microglial immune training affects PD remain unknown.

The innate immune system consists of a series of conserved pattern recognition receptors (PRRs) that detect and respond to pathogen-associated molecular patterns (PAMPs). The broad spectrum of PRRs allows the host to recognize and rapidly defend against a large number of pathogens[22]. Inflammasomes are a class of cytoplasmic multi-protein complex PRRs[23]. In response to infection or tissue damage, pattern recognition receptors [Nod-like receptor (NLR) or non-NLR sensor proteins], adaptor proteins (apoptosis-associated speck-like protein containing a C-terminal caspase recruitment domain, ASC), and inflammatory caspases assemble into an oligomeric structure[23,24]. Gasdermin D

(GSDMD) is activated by inflammatory caspases which release its active N-terminal fragment (p30), and oligomerizes to form transmembrane pores that induce pyroptosis[25]. Inflammasome-induced pyroptosis has been widely reported to play a critical role in bacterial infection-triggered inflammation. Typically, LPS from Gram-negative bacteria can activate the NLRP3-induced canonical inflammasome pathway, which leads to GSDMD-dependent release of pro-inflammatory cytokines, including IL-1β and IL-18[25−28]. However, the role of inflammasomes and pyroptosis playing in CNS immune training and how this process affects PD is unknown.

Here, we report that LPS-induced NLRP3 and GSDMD activation in peripheral myeloid cells contributes to the immune training of microglia. NLRP3 and GSDMD dependent immune training of microglia facilitates neuroinflammation and progressively exacerbates the pathological effects of experimental PD.

2. Materials and methods

2.1. Animals

$Gsdmd^{-/-}$ mice with C57BL/6 genetic background were gifts from Dr. Feng Shao (National Institute of Biological Sciences, Beijing, China). $Nlrp3^{-/-}$ mice came from the Laboratory Animal Center of Southeast University (Nanjing, China). $Nlrp3^{fl/fl}$ mice were obtained from Nanjing University Laboratory Animal Center (Nanjing, China). The A30P mice (expressing human mutant A30P α-syn under the control of the Thy-1 promoter) were a gift from Dr. Jiawei Zhou (Chinese Academy of Sciences, China). The $Gsdmd^{fl/fl}$ mice were generated using conditional gene targeting methods by Biocytogen. Myeloid cells-conditional NLRP3 or GSDMD KO mice ($Nlrp3^{fl/fl}Lysm^{Cre}$ or $Gsdmd^{fl/fl}Lysm^{Cre}$) and microglia-conditional GSDMD KO mice ($Gsdmd^{fl/fl}Cx3cr1^{CreERT2}$) were generated as previously described[29]. The mice were maintained under pathogen-free conditions and on a 12 h light/dark cycle at 25 °C with food and water available *ad libitum*. All mice were kept in a barrier facility, and all animal experiments were conducted in accordance with the procedure approved by the Ethical Review Committee for Laboratory Animal Welfare of the Nanjing Medical University and Nanjing University of Traditional Chinese Medicine.

2.2. Peripheral inflammatory stimulation and MPTP model

2−3-Month-old mice were randomly assigned to vehicle or treatment groups. The vehicle group was intraperitoneally (i.p.) injected with PBS, and treatment groups received bacterial LPS (from *Escherichia coli* 0111: B4, Sigma−Aldrich) injection at a dose of 0.5 mg per kg body weight for a single day ($1 \times$ LPS) or two consecutive days ($2 \times$ LPS). The blood and brain samples were collected at 3 h post-injection. MPTP-HCl induced mouse model was established as previously described[30]. In brief, the mice were administered an i.p. injection of 20 mg/kg 4 times at 2 h intervals. Mice were sacrificed for analysis 7 days later. For IL-1β antibody administration, age-matched male WT and $Gsdmd^{-/-}$ mice ($n = 3$ mice per group) were intraperitoneally injected with anti-IL-1β antibody (4 mg/kg, Bio X Cell, BE0246). After 1 h, the mice were injected with LPS (0.5 mg/kg), then treated with anti-IL-1β antibody again at 6 h after LPS treatment. Then the mice were subjected to an MPTP-induced PD model.

2.3. Bone marrow chimeras

The recipient mice were subjected to lethal-dose irradiation (10 Gy), and 24 h later, bone marrow cells (1×10^7) from the donor mice were i.v. injected into lethally irradiated mice. Under these conditions, the radio-resistant CNS-resident cells can be retained; however, bone marrow and peripheral blood cells would be replaced by bone marrow cells from donor mice. After 8 weeks, the chimeric mice can be subjected to further study.

2.4. Cell culture

BV2 cells were cultured in DMEM supplemented with 10% (v/v) fetal bovine serum (FBS), 100 mg/mL penicillin G and 100 mg/mL streptomycin. For primary microglia, cerebral cortices from neonatal mice at 1−3 days were collected and carefully stripped of their blood vessels and meninges, and then the tissues were digested with 0.25% trypsin−EDTA. Following the digestion, the single-cell suspensions were obtained by passing through a cell strainer (70 μm). The cell suspensions were seeded into poly-D-lysine-pre-coated flasks and cultured in DMEM/F12 supplemented with 10% FBS, 100 mg/mL penicillin G, and streptomycin at 37 °C and 5% CO_2. The medium was replaced every 4−5 days. After 10−14 days, microglia were separated from the underlying astrocytic layer by gentle shaking of the flask and were seeded in poly-D-lysine-pre-coated plates for further study.

2.5. Immunohistochemistry and immunofluorescence staining

Mice were anesthetized and perfused with 4% paraformaldehyde. Brains were extracted, dehydrated in 30% sucrose solution, embedded in OCT, and continuously sliced at 25 μm thickness. The immunohistochemistry staining was processed as previously described[31]: tissue sections were blocked with 3% H_2O_2 for 15 min and 5% goat serum for 30 min at room temperature after heat-induced antigen retrieval. The sections were then incubated with primary antibody to TH (1:500, AB152, Merck-Millipore) at 4 °C for 12 h and followed by incubating with horseradish peroxidase (HRP)-labeled goat anti-rabbit (1:300; 31460, ThermoFisher Scientific). The number of TH-positive cells in the SN area was determined by stereological methods, as previously described[32]. For immunofluorescence staining: tissue sections were blocked with 5% goat serum for 30 min at room temperature and were incubated with primary antibodies to IBA1 (1:500, 019-19741, Wako) and GFAP (1:500, G3893, Sigma−Aldrich) at 4 °C for 12 h. The sections were then incubated with fluorescent-labeled goat anti-rabbit (1:500, 111-545-144, Jackson ImmunoResearch) and goat anti-mouse (1:500, 115-165-075, Jackson ImmunoResearch). The related fluorescence intensities were analyzed by image pro plus software.

2.6. Western blot analysis

Spleen and brain SN specimens were quickly collected on ice and homogenized 1:10 (w/v) in NP-40 lysis buffer (50 mmol/L Tris-HCl, pH 7.4, containing 150 mmol/L NaCl, 1% [v/v] Igepal, 10% [w/v] glycerol, 50 mmol/L NaF, 1 mmol/L Na_3VO_4, 1 mmol/L dithiothreitol and 1 mmol/L phenylmethylsulphonyl fluoride) supplemented with protease inhibitor cocktail. For in vitro experiments, cells were collected in NP-40 lysis buffer containing protease inhibitor cocktail. The protein lysates were centrifuged at $12,000 \times g$ for 10 min, and the protein concentrations were detected by PierceMT BCA protein assay. Then the protein samples were resolved by SDS-PAGE, transferred to nitrocellulose membranes, and subjected to appropriate antibodies. The following primary antibodies were used: anti-AIM2 (1:3000, 13095s, Cell Signaling Technology); anti-NLRC4 (1:500, Santa Cruz Biotechnology, sc-49395); anti-phosphorylated α-synuclein (1:1000, 015-25191, Wako); anti-α-synuclein (1:1000, ab51253, Abcam); anti-GSDMD (1:1000, ab2019845, Abcam); anti-NLRP3 (1:3000, AG-20B0014, AdipoGen); anti-caspase-1 (1:1000, AG-20B-0042, AdipoGen); anti-IL-1β (1:1000, AF-401-NA, R&D Systems); anti-β-actin (1:5000, A1978, Sigma−Aldrich). The membrane was washed and incubated for 1 h at room temperature with the corresponding secondary antibodies: IRDye 680RD-anti-mouse (1:5000, 926-68070, LI-COR Biosciences); IRDye 800CW-anti-rabbit (1:5000, 926-32211, LI-COR Biosciences); anti-mouse-HRP (1:3000, 31340, ThermoFisher Scientific); anti-goat-HRP (1:3000, 31402, ThermoFisher Scientific). Immunoreactivity was visualized by the Odyssey Imaging System (LI-COR Biosciences) or enhanced chemiluminescence.

2.7. Flow cytometry

Anesthetized mice were perfused with ice-cold PBS. The whole brain tissues were isolated and homogenized on ice. Brain homogenates were digested in DMEM/F12 containing 20 U/mL DNAse I (Sigma−Aldrich, D5025) and 100 U/mL collagenase IV (ThermoFisher Scientific, 17104019), shaking at 250 rpm for 1 h, and then washed and filtered through a 70 μm cell strainer. The monocytes were isolated by a discontinuous Percoll gradient. Purified cells were incubated with mixed antibodies for 30 min at 4 °C as follows: the Fc receptor blocking antibody CD16/CD32 (BD Bioscience, 553141, 1:100), CD11b-APC (eBioscience, 17-0112-82, 1:400), CD45-FITC (eBioscience, 11-0451-85, 1:400), and incubated for 30 min at 4 °C. Cells were washed again and resuspended in PBS for flow cytometry (FACS) measurement by flow cytometry using a Citole S (Beckman Coulter) and analyzed using FlowJo (BD Bioscience).

2.8. Quantitative polymerase chain reaction (qPCR) analysis

Total RNA extraction, cDNA synthesis, and qPCR reactions were performed according to the manufacturer's instructions. TRIzol reagent (Invitrogen) was used to extract RNA from SN tissues of the brain or primary microglia, and RNA was used for subsequent cDNA synthesis. Quantitative RT-PCR was performed using SYBR Green Supermix (Vazyme). The primers used in this study are provided in Table S1.

2.9. Enzyme-linked immunosorbent assay (ELISA)

Serum cytokine values were determined by ELISA. Serum was obtained by coagulation of whole blood for 30 min at room temperature and centrifugation at $600 \times g$ firstly for 30 min at room temperature and then at $13,800 \times g$ for 10 min at 4 °C. For brain cytokines measurement, brain homogenates were centrifuged at $13,800 \times g$ for 30 min at 4 °C. Protein levels were normalized against the total protein amount as measured by the BCA protein assay. All samples were diluted into appropriate concentrations based on the standard curves and measured by ELISA (murine IL-

1β, DY401; mouse IL-6, DY406; murine TNF-α, DY410; all kits from R&D Systems) according to the manufacturer's protocol.

2.10. RNA-seq analysis

For RNA-seq, microglia from mice were collected on Day 2 after $1 \times$ LPS stimuli. Total RNA isolation, cDNA library construction, and RNA-seq were performed with the BGISEQ-500 system (Beijing Genomic Institution). Clean reads were mapped to the mouse genome (GRCm38.p5) by HISAT2. The matched reads were calculated and then normalized to FPKM. The fold change for all possible comparisons was calculated, and a 1.5-fold cut-off was used to select genes with expression changes. KEGG pathway analysis and GO-BP analysis were performed using the R package on expressed genes that were significantly different from target genes. The sequencing data have been deposited in the NCBI Sequence Read Archive database under the NCBI Bio project PRJNA887688.

2.11. ATAC-seq analysis

ATAC-seq was performed as previously reported[33]. In brief, 20,000 microglia were washed once with PBS and resuspended in 50 μL lysis buffer (10 mmol/L Tris-HCl, 10 mmol/L NaCl, 3 mmol/L MgCl$_2$, 1% Tween-20, 1% NP-40, 0.01% digitonin) to isolate nuclei. The suspension of nuclei was centrifuged at $500 \times g$, 4 °C for 5 min, followed by resuspended in 20 μL transposition reaction mix (10 μL 5 × TTBL, 5 mL TTE Mix V50 and 35 μL nuclease-free H$_2$O) of TruePrep DNA Library Prep Kit V2 for Illumina (TD502, Vazyme). Samples were then PCR amplified and incubated at 37 °C for 30 min. DNA was isolated using VAHTSTM DNA Clean Beads (N411, Vazyme). ATAC-seq libraries were first subjected to 18 cycles of pre-amplification and then purified with VAHTSTM DNA Clean Beads. Library concentration was measured using a Qubit dsDNA HS Assay Kit (Invitrogen, Q32854) according to the manufacturer's instructions. The ATAC library was sequenced on an Illumina Hiseq-Xten PE150 by Novogene to generate 2×150-bp paired-end reads.

Nextera adaptor sequences were first trimmed from the reads using a skewer (0.2.2). These reads were aligned to a reference genome using BWA with standard parameters. These reads were then filtered for high quality (MAPQ 13), non-mitochondrial chromosome, and properly paired reads (longer than 18 nt). All peak calling was performed with macs2 using 'macs2 callpeak–nomodel–keepdup all–call-summits'. For simulations of peaks called per input read, aligned and de-duplicated BAM files were used without any additional filtering. The sequencing data have been deposited in the NCBI Sequence Read Archive database under the NCBI Bio project PRJNA888443 (ATAC-Seq).

2.12. Behavioral assessments

2.12.1. Open field test
The open field test was conducted before all other behavioral tests, as previously described[34,35]. Briefly, the device is made of white plastic (50 cm × 50 cm), and the area is divided into a peripheral area and a central area, each of which occupies 50% of the total open area. About 1 h before the experiment, the mice were transferred to the laboratory for adaptability testing and then placed into the open field device under evenly distributed low light for 15 min. During the test, the total travel distance and the duration of the central area were automatically recorded.

2.12.2. Pole test
A Pole test was used to evaluate the balance and coordination ability of mice, as previously described[34]. Briefly, a 0.5 m long and a diameter of 1 cm pole was placed vertically into the cage, and the mouse was placed at the top. The total time from the top to descend back into the cage was recorded. Before the test day, each mouse experienced 5 consecutive training trials with 30 min intervals between each training. On the test day, each mouse was tested 3 times at 3 min intervals, and the average value of the 3 times was taken as the data.

2.12.3. Accelerating rotarod test
The accelerating rotarod test was conducted as previously described[36]. Briefly, mice were acclimated to the rotarod apparatus, which accelerates from 5 to 30 rpm in 300 s, and the latency to fall off was recorded. Before the test, each mouse was trained over 3 consecutive days with 5 trials per day at 30 min intervals. On the test day, 5 trials were conducted at 3 min intervals, and the average time of the latency to fall was recorded.

2.12.4. Hindlimb clasping test
The mice were suspended by their tails and videotaped for 15 s. The score of hindlimb was rated from 0 to 3 according to severity: 0 = hindlimbs splayed outward and away from the abdomen; 1 = one hindlimb retracted inward toward the abdomen for at least 50% of the observation period; 2 = both hindlimbs partially retracted inward toward the abdomen for at least 50% of the observation period; and 3 = both hindlimbs completely retracted inward toward the abdomen for at least 50% of the observation period. A score of 0.5 was utilized when appropriate. Scores were averaged for three independent trials during three consecutive days.

The videos were stacked into frames using Photoshop software (Adobe). All the layers were converted to a smart object and then set into the stack mode "maximum" to capture the paws and to sum the hindlimb movements in a single frame image. The percentage area of hindlimb coverage, which was inverted for clarity, was evaluated by ImageReader software (Fujifilm) pixel intensity measurement.

2.12.5. Wire hang test
Mice were hanged on the lowest area of the metal mice covered 30 cm over the ground, and tested for their ability to hold. The maximal duration time was set to 90 s to avoid exhaustion. The latency to fall was recorded, and the test was performed three times separated by 30 min intervals.

2.13. Statistical analysis

Data are expressed as the means $\pm$ standard error of the mean (SEM). Statistical analysis was performed with GraphPad Prism 7.0 software using unpaired t-tests for two groups and multiple unpaired t-tests for multiple groups. A P value below 0.05 was considered statistically significant (*$P < 0.05$, **$P < 0.01$, and ***$P < 0.001$).

3. Results

3.1. Inflammasome-mediated pyroptosis is involved in the periphery infection-induced CNS innate immune training

To evaluate whether the NLRP3 inflammasome and pyroptosis are involved in peripheral bacterial infection-induced CNS innate immune training, we administered low-dose LPS by IP injection to mice on two consecutive days to mimic peripheral bacterial infection[21]. Serum pro-inflammatory cytokines were significantly increased after the first injection and reduced upon the second dose of LPS (Fig. 1A, Supporting Information Fig. S1A). By detecting protein levels of different inflammasomes in the spleen, we found that NLRP3 expression was significantly increased after the first injection, and decreased in response to the second dose of LPS. The protein level of AIM2 and NLRC4 did not change (Fig.
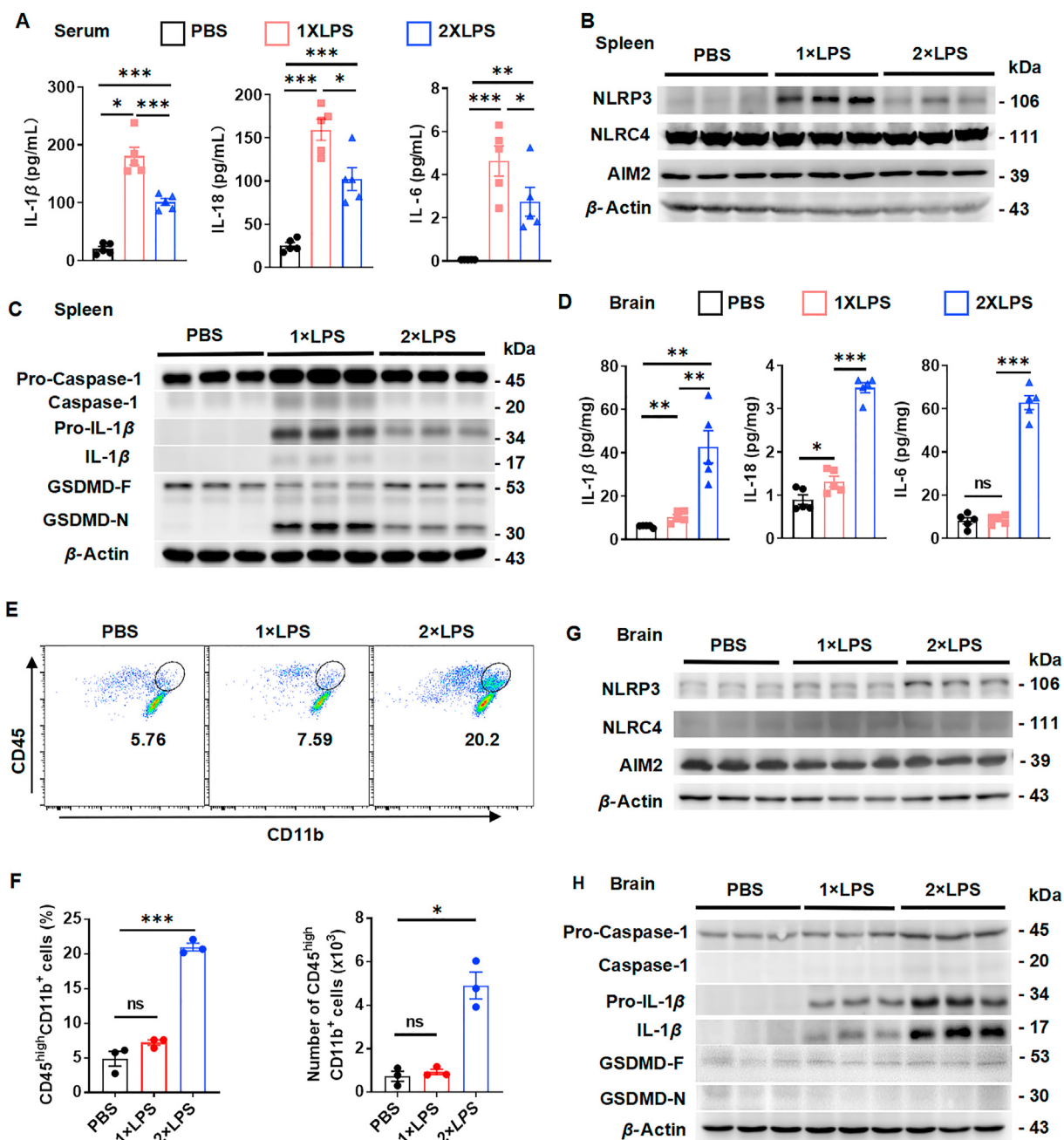

Figure 1 Innate immune memory formation in periphery and central nervous system (CNS) upon lipopolysaccharide (LPS) stimuli. (A) ELISA analysis of IL-1β, IL-18, and IL-6 in serum from mice after PBS, 1 × LPS, or 2 × LPS treatment (*n* = 5 per group). (B) Immunoblot analysis of NLRP3, NLRC4, AIM2 and β-actin (loading control) in spleen from mice in (A). (C) Immunoblot analysis of caspase-1, IL-1β, GSDMD, and Actin (loading control) in spleen. (D) ELISA analysis of IL-1β, IL-18, and IL-6 in brain; (E, F) Flow cytometric analysis of activated microglia (CD11b $^+$ CD45^{high}) in brain tissue. Data are shown as representative plots (E) and quantified percentages and cell numbers (F) (*n* = 3 per group). (G) Immunoblot analysis of NLRP3, NLRC4, AIM2, and β-actin (loading control) in brain tissue. (H) Immunoblot analysis of caspase-1, IL-1β, GSDMD, and β-actin (loading control) in brain tissue. Data shown are mean ± SEM; *$P < 0.05$, **$P < 0.01$, ***$P < 0.001$ for one-way ANOVA.
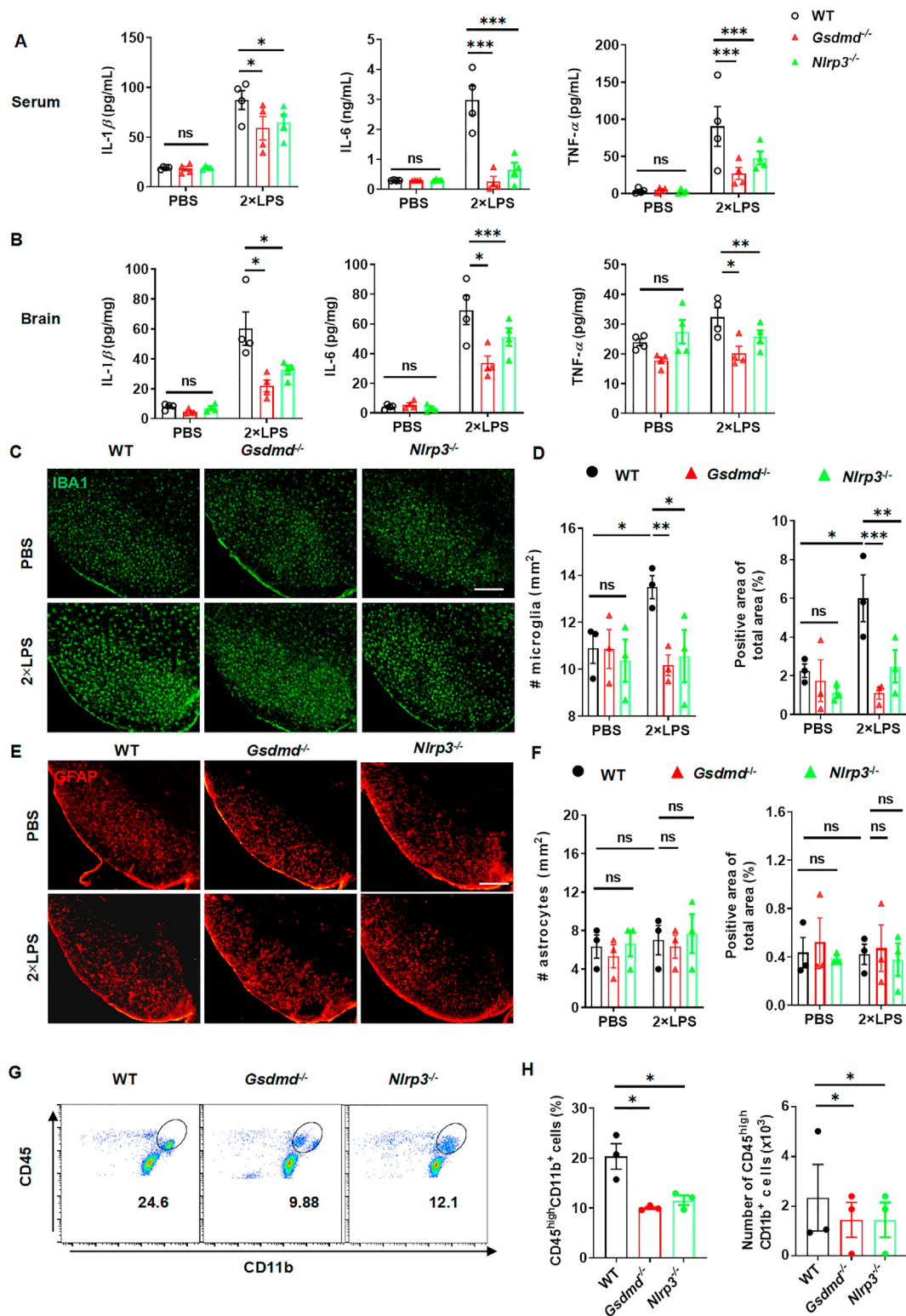
Figure 2 Deficiency of NLRP3 or GSDMD inhibits CNS innate immune training and neuroinflammation. (A, B) ELISA analysis of IL-1β, IL-6, and TNF-α in serum (A) and brain (B) from WT, *Gsdmd*$^{-/-}$ and *Nlrp3*$^{-/-}$ mice upon PBS or 2 × LPS injection (n = 4 per group). (C, D) Immunofluorescence analysis of microglia (IBA1) in brain substantia nigra (SN) tissue from WT, *Gsdmd*$^{-/-}$ and *Nlrp3*$^{-/-}$ mice upon PBS or 2 × LPS treatment. Data are shown as representative pictures (C), quantified cell numbers, and positive area (D) (n = 3 per group). Scale bar, 200 μm. (E, F) Immunofluorescence analysis of astrocyte (GFAP) in brain SN tissue from mice in (C)−(D). Data are shown as representative pictures (E), quantified cell numbers, and positive area (F) (n = 3 per group). Scale bar, 200 μm. (G, H) Flow-cytometric analysis of activated microglia (CD11b$^+$ CD45^{high}) in brain tissue from WT, *Gsdmd*$^{-/-}$ and *Nlrp3*$^{-/-}$ mice upon 2 × LPS treatment. Data are shown as representative plots (G), quantified percentages, and cell numbers (H) (n = 3 per group). Data are representative of three independent experiments; *P < 0.05, **P < 0.01, ***P < 0.001 for one-way ANOVA. Data shown are mean ± SEM.
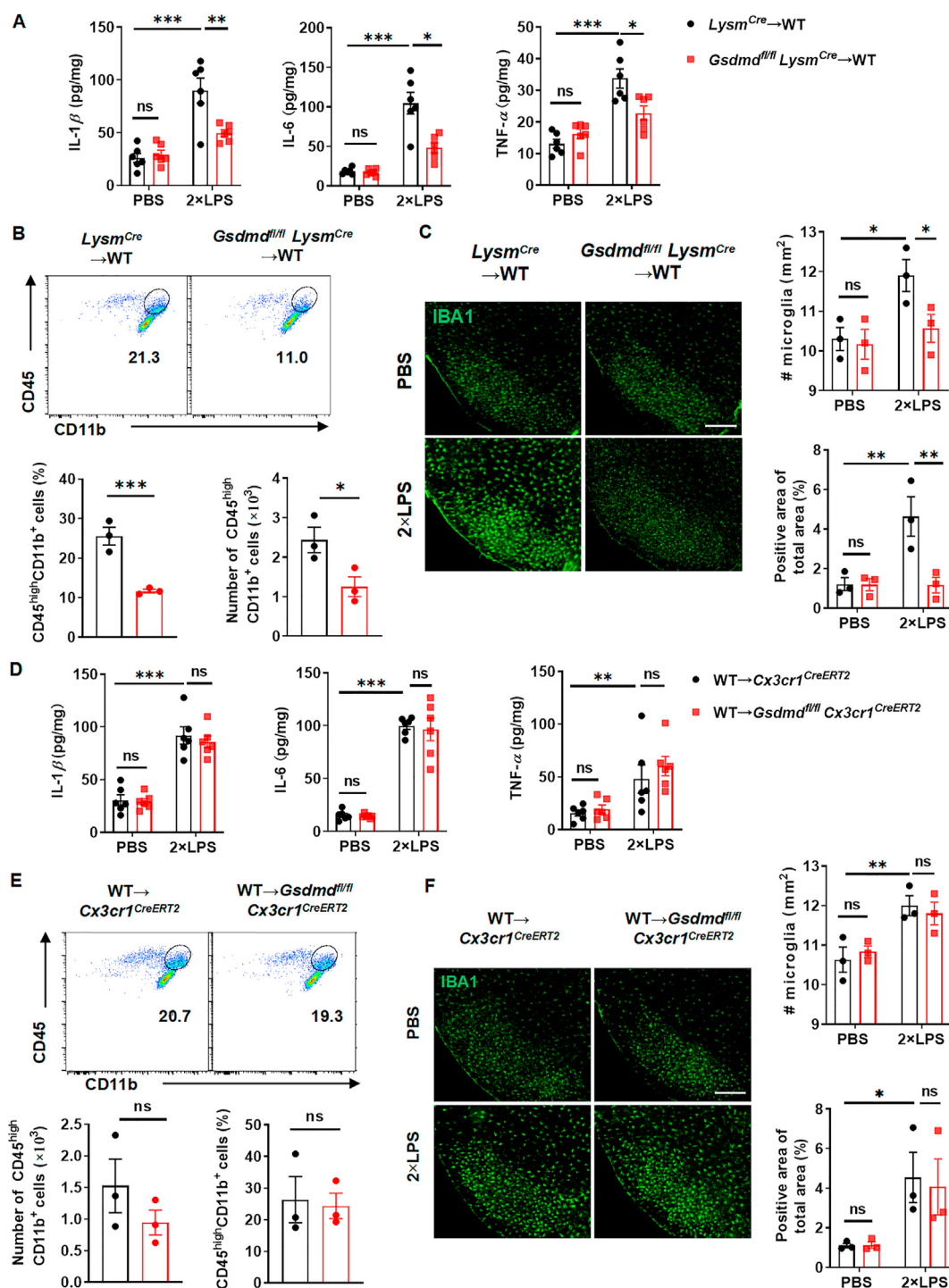
Figure 3 GSDMD in peripheral myeloid cells promotes CNS inflammation under LPS stimuli. (A) ELISA analysis of IL-1β, IL-6, and TNF-α in brain of indicated chimeric mice upon PBS or 2 × LPS treatment. (n = 6 per group). (B) Flow-cytometric analysis of activated microglia (CD11b^{+} CD45^{high}) in brain tissue from indicated chimeric mice upon PBS or 2 × LPS treatment. Data are shown as representative plots (upper), and quantified percentages and cell numbers (lower) (n = 3 per group). (C) Immunofluorescence analysis of IBA1 in brain SN tissue from indicated chimeric mice upon PBS or 2 × LPS treatment. Data are shown as representative pictures (left), and quantified cell numbers and positive area (right) (n = 4 per group). Scale bar, 200 μm. (D) ELISA analysis of IL-1β, IL-6, and TNF-α in brain of indicated chimeric mice upon PBS or 2 × LPS treatment (n = 6 per group). (E) Flow-cytometric analysis of activated microglia (CD11b^{+} CD45^{high}) in brain tissue from indicated chimeric mice upon PBS or 2 × LPS treatment. Data are shown as representative plots (upper) and quantified percentages and cell numbers (lower) (n = 3 per group). (F) Immunofluorescence analysis of IBA1 in brain SN tissue from indicated chimeric mice upon PBS or 2 × LPS treatment. Data are shown as representative pictures (left) and quantified cell numbers and positive area (right) (n = 3 per group). Scale bar, 200 μm. Data are representative of three independent experiments. Data shown are mean ± SEM; *P < 0.05, **P < 0.01, ***P < 0.001 (unpaired t-test).
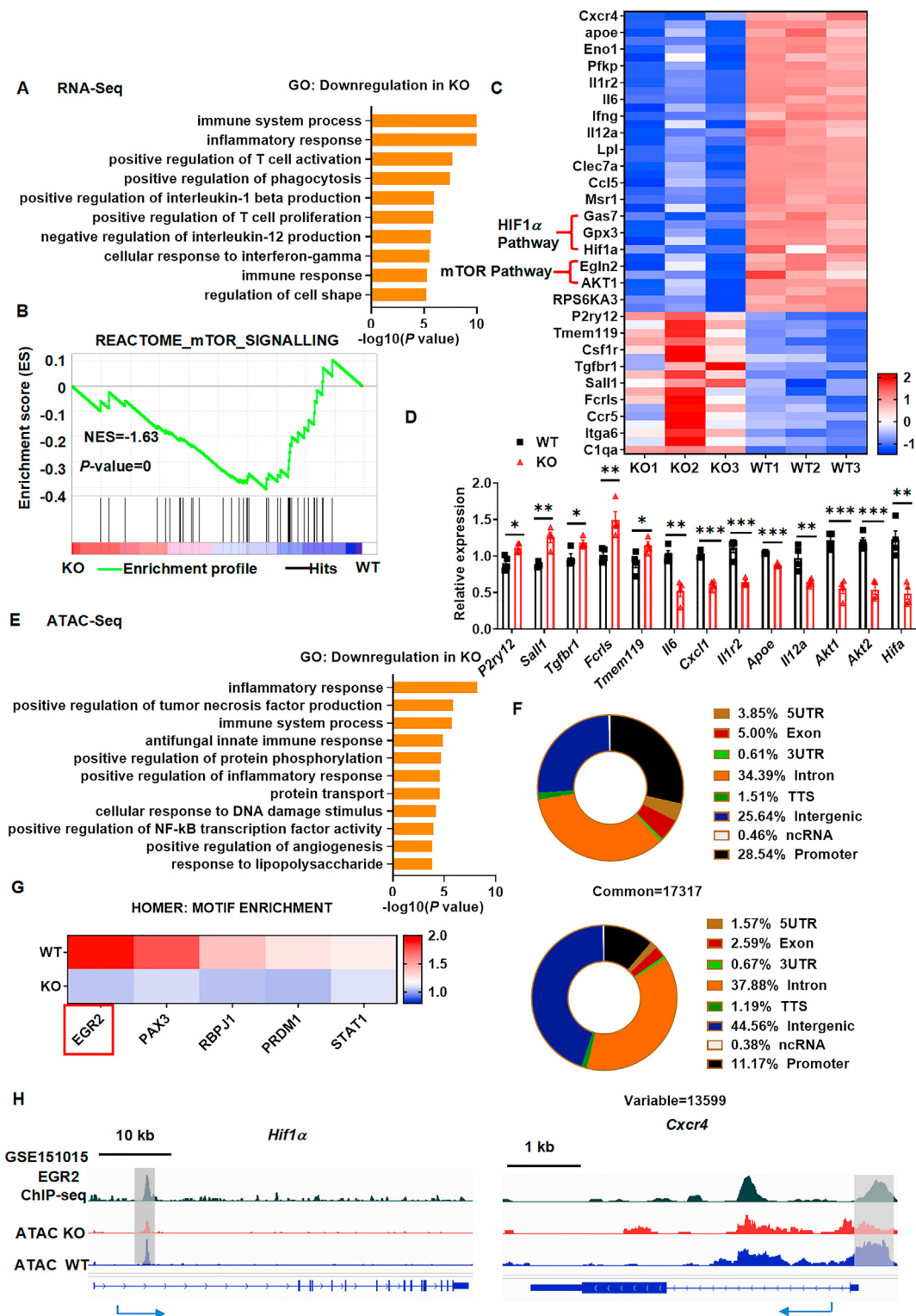
Figure 4 Epigenetic and transcriptional changes in GSDMD deficiency mice upon LPS stimuli. (A) WT and *Gsdmd*$^{-/-}$ mice were treated with $1 \times$ LPS for 48 h, and microglia were then sorted to perform RNA-seq. GO-BP analysis shows the most significantly down-regulated genes of signaling pathways in microglia from *Gsdmd*$^{-/-}$ mice using RNA-seq data. (B) GSEA for the enrichment of the "mTOR signaling pathway" using the Reactome database in microglia sorted from WT and *Gsdmd*$^{-/-}$ mice. (C) The heatmap of genes with adjusted *P*-value < 0.05, false discovery rate < 0.05, and fold-change >1.5 from RNA-seq analysis of microglia from WT and *Gsdmd*$^{-/-}$ mice. (D) Quantitative PCR analysis of indicated genes in microglia from mice in (A). Data were normalized to the reference gene *Hprt*. (E) WT and *Gsdmd*$^{-/-}$ mice were treated with $1 \times$ LPS for 48 h, and subsequently microglia were sorted to perform ATAC-seq. Pie charts visualize the distribution of ATAC-seq peaks that are shared between microglia from WT and *Gsdmd*$^{-/-}$ (common) or peaks specific to microglia from WT or *Gsdmd*$^{-/-}$ (variable) across the genome [five

1B, Fig. S1B). Consistently, enhanced cleavage of caspase-1, IL-1β, and GSDMD was observed after the first dose of LPS followed by a reduction in response to the second dose of LPS (Fig. 1C, Fig. S1C). Thus, NLRP3 and GSDMD-dependent pyroptosis is activated in response to peripheral LPS. In sharp contrast, pro-inflammatory cytokines in the brain were significantly increased when mice were administered the second dose of LPS (Fig. 1D, Fig. S1A), indicating that immune training in brain resident cells occurred following the first exposure to LPS. In addition, FACS analysis on brain tissue showed enhanced microglial activation (CD45^{high} CD11b$^+$) in response to the second dose of LPS (Fig. 1E and F). These data indicate that microglia undergo training in response to peripheral LPS. Although the expression of NLRP3, pro-caspase1, pro-IL-1β and IL-1β was elevated, the cleavage of caspase-1 and GSDMD did not change following the second dose of LPS (Fig. 1G and H, Fig. S1B and S1C). These results suggest that the NLRP3 inflammasome was not activated in the CNS. The increased expression of NLRP3 was likely due to the enhanced transcript levels of increased inflammatory signal. However, the increased expression of pro-IL-1β and mature-IL-1β was likely a consequence of periphery transfer. Thus, NLRP3 and GSDMD activity in the CNS did not directly regulate the training of microglia. The Perls' Prussian blue staining, which detects the presence of blood iron in the brain, and the Evans blue staining, which measures BBB permeability, were performed to evaluate the integrity of the BBB (Fig. S1D). In line with the previous studies, a low dose of LPS did not affect BBB permeability[21]. These data indicate that NLRP3 and GSDMD activity in peripheral cells outside the CNS promotes immune training of microglia in the CNS. Thus, we next assessed microglial training in NLRP3 and GSDMD deficient mice.

3.2. GSDMD is essential for peripheral stimulation-induced CNS immune training and inflammation

To further verify the essential role of peripheral NLRP3 and GSDMD-induced pyroptosis on CNS immune training, we administered two doses of LPS to WT, Nlrp3$^{-/-}$ and Gsdmd$^{-/-}$ mice (to induce CNS inflammation according to the results in Fig. 1). Interestingly, NLRP3 or GSDMD deficient mice were resistant to LPS-induced inflammatory phenotypes in both periphery and CNS. Deletion of NLRP3 or GSDMD significantly reduced the levels of IL-1β, TNF-α, and IL-6 in both serum and brain tissue (Fig. 2A and B). Furthermore, microglia activation, numbers of IBA-1 positive cells and total positive area in the midbrain of Nlrp3$^{-/-}$ and Gsdmd$^{-/-}$ mice were significantly reduced when compared to WT mice (Fig. 2C and D). Whereas activated astrocytes (GFAP positive cells) showed no discrepancy between WT, Nlrp3$^{-/-}$, and Gsdmd$^{-/-}$ mice after two LPS challenges (Fig. 2E and F). Consistently, FACS analysis also revealed a reduction in microglia activation in Nlrp3$^{-/-}$ and Gsdmd$^{-/-}$ mice compared to WT mice after two doses of LPS (Fig. 2G and H). Taken together, we conclude that NLRP3 or

GSDMD deficiency attenuates peripheral LPS-induced CNS immune training and inflammation.

3.3. GSDMD in peripheral myeloid cells contributes to the formation of CNS immune training

To determine if NLRP3 and GSDMD directed immune training in the CNS is mediated by peripheral cells or CNS-resident cells, we performed bone marrow transplantations to compare the effects of CNS-resident cells and peripheral immune cells on CNS immune memory. We transferred the bone marrow cells of CD45.1 donor mice into CD45.2 receipt mice to confirm the success of reconstitution. The FACS analysis showed that the blood from recipients (CD45.2) was completely replaced by donor mice (CD45.1) (Supporting Information Fig. S2A), suggesting the bone marrow transplantation experiments were successful. As expected, WT mice that received Nlrp3$^{-/-}$ or Gsdmd$^{-/-}$ bone marrow showed a reduction in IL-1β, IL-6, and TNF-α in the brain after two doses of LPS compared to mice receiving WT bone marrow (Fig. S2B). However, comparable production of pro-inflammatory cytokines was observed between WT and Nlrp3$^{-/-}$, or Gsdmd$^{-/-}$ mice reconstituted with WT bone marrow (Fig. S2B). As demonstrated by immunofluorescence (Fig. S2C and S2D), we also observed fewer activated microglia cells in mice receiving Nlrp3$^{-/-}$ or Gsdmd$^{-/-}$ bone marrow than in mice receiving WT bone marrow, irrespective of the recipient genotypes. Similarly, microglia activation was reduced in mice reconstituted with Nlrp3$^{-/-}$ or Gsdmd$^{-/-}$ bone marrow (Fig. S2E and S2F). Thus, these results indicate that NLRP3 or GSDMD in the periphery is indispensable for peripheral stimulation of inflammation and immune training in the CNS.

GSDMD is known to be highly expressed in innate immune myeloid cells, including microglia, comparatively to lymphocytes and other CNS cell types[29]. In light of our results, we speculated that GSDMD mainly functions in peripheral myeloid cells. To verify our hypothesis, we established WT bone marrow chimeric mice reconstituted with Gsdmd$^{fl/fl}$Lysm^{Cre} or Lysm^{Cre} bone marrow cells. GSDMD deficiency in peripheral myeloid cells significantly attenuated the levels of IL-1β, TNF-α, and IL-6 in the brain following two doses of LPS (Fig. 3A). In addition, activation of microglia was blocked in mice reconstituted with Gsdmd$^{fl/fl}$Lysm^{Cre} bone marrow. Further, the number of CD45^{high} CD11b$^+$ cells was also markedly decreased (Fig. 3B and C). Thus, GSDMD in peripheral myeloid cells is an essential mediator of LPS-induced neuroinflammation. In support of our findings, Gsdmd$^{fl/fl}$Cx3cr1^{CreERT2} (tamoxifen-induced Cre expression specific deletion of GSDMD in long-lived microglia) or Cx3cr1^{CreERT2} control mice, reconstituted with WT bone marrow, did not ameliorate the production of pro-inflammatory cytokines or microglial activation, following two doses of LPS injection (Fig. 3D and F). Collectively, these results demonstrate that GSDMD activation in peripheral myeloid cells is required for neuroinflammation and immune training of microglia in response to LPS.

---

prime untranslated regions (5′ UTR), Exon, three prime untranslated regions (3′ UTR), Intron, transcription termination site (TTS), Intergenic, noncoding RNA (ncRNA), and Promoter] (n = 3/group). (F) GO-BP analysis shows the most significantly down-regulated genes in microglia from Gsdmd$^{-/-}$ mice-related signaling pathways from ATAC-seq. (G) Heat maps display the enrichment of TF motifs in ATAC-seq peaks of microglia from WT and Gsdmd$^{-/-}$ mice. (H) Genome track view of Hif1a and Cxcr4 loci show ATAC-seq for microglia from WT and Gsdmd$^{-/-}$ mice and EGR2 ChIP-seq peaks (GSE151015; from BMDMs after IL-4 treatment). Gray boxes highlight notable differences in chromatin accessibility. Note, the open chromatin region is defined as a genomic region with differential chromatin accessibility of $|\log_2(KO/WT)| \geq 2$ and $|\log_2(KO/WT)| \geq 1$ adjusted $P \leq 0.05$ as a cut-off. Data shown are mean ± SEM; *$P < 0.05$, **$P < 0.01$, ***$P < 0.001$ (unpaired t-test).

3.4. GSDMD deficiency attenuates the epigenetically changes in microglia through IL-1β signaling during peripheral stimulation

Microglia activity has been previously attributed to mediate immune training in the brain[21]. Consistently, the activation of microglia (IBA-1 positive cells) was observed in the midbrain of mice after a single dose of LPS. However, astrocytes (GFAP-positive cells) displayed a quiescent state (Supporting Information Fig. S3A and S3B). To further dissect the specific mechanism of GSDMD in microglial immune training, we performed RNA-seq on microglia from WT and *Gsdmd*$^{-/-}$ treated mice using a single dose of LPS. Principal component (PC) analysis showed that the expression profiles of microglia from WT mice had a distinct gene clustered architecture when compared with the microglia population from *Gsdmd*$^{-/-}$ mice (Fig. S3C). Gene ontology biological process (GO-BP) analysis indicated that down-regulated genes in microglia from GSDMD knockout mice were related to immune system processes and inflammatory responses (Fig. 4A). Gene Set Enrichment Analysis (GSEA) revealed that the mTOR pathway was significantly down-regulated in microglia from GSDMD knockout mice in both Reactome and Hallmark gene sets, although it was not ranked in the top down-regulated pathway (Fig. 4B, Fig. S3D and S3E). The heatmap of RNA-seq analysis revealed that differentially expressed genes in microglia from GSDMD knockout mice were related to the microglia activation state. Indeed, disease-associated microglia (DAM) signature genes, such as *Apoe*, *Cxcl1*, *Il12a*, and *Il6*, were down-regulated, whereas expression of genes associated with homeostatic microglia, such as *P2ry12*, *Sall1*, *Tgfbr1*, and *Tmem119* was increased (Fig. 4C). Notably, several genes involved in mTOR and the HIF1a signaling pathways, such as *Akt1*, *Akt2*, *Hif1a*, *Egln1*, and *Egln2*, were downregulated in GSDMD knockout microglia (Fig. 4C). The mTOR and HIF1α pathway is essential for the induction of immune training in microglia and peripheral myeloid cells[21,37]. Real-time PCR analysis confirmed these changes (Fig. 4D). Consistently, we observed similar changes in microglia from *Gsdmd*$^{fl/fl}$/*Lysm*^{Cre} and *Nlrp3*$^{fl/fl}$/*Lysm*^{Cre} mice, compared to those of *Lysm*^{Cre} mice (Fig. S3F). It has been reported that the transcriptional changes underpinning innate immune training in the brain, resulting from epigenetic alterations of microglia[21]. Therefore, we performed transposase-accessible chromatin with sequencing (ATAC-seq) on microglia from WT and *Gsdmd*$^{-/-}$ mice treated with LPS. When compared to common open chromatin sites, microglial unique open chromatin sites from WT or *Gsdmd*$^{-/-}$ were more enriched in intergenic regions and less likely to be detected at promoter regions (Fig. 4E). GO analysis further confirmed the top biological processes down-regulated in microglia from *Gsdmd*$^{-/-}$ mice were inflammatory responses and immune system processes (Fig. 4F). When compared to WT, open chromatin regions in microglia from *Gsdmd*$^{-/-}$ mice were less enriched for several TF motifs associated with inflammatory response, such as EGR2, PAX3, RBPJ1, PRDM1, and STAT1, compared to those in WT microglia (Fig. 4G). We performed the combined analysis of ATAC-seq and public Chip-seq (GSE151015) data which revealed that EGR2 binding sites were in the differential peak, and predominantly in the +1 kb promoter region of *Cxcr4*. For *Hif1a*, the differential peak intensity is found at the site of EGR2 binding in the first intronic enhancer region (Fig. 4H). These findings collectively demonstrated that GSDMD in peripheral myeloid cells is essential for the formation of immune training in microglia due to epigenetic and transcriptional changes.

IL-1β release depends on the formation of GSDMD pores in the plasma membrane[38]. IL-1β also has been reported to induce activation of the mTOR signaling pathway[39,40]. In addition, GO-BP showed that inflammatory pathways, such as the IL-1β receptor pathway, were significantly decreased in microglia from *Gsdmd*$^{-/-}$ mice (Fig. 5A). Thus, we speculated that GSDMD in peripheral myeloid cells promotes neuroinflammation through the release of IL-1β, which activates IL-1R on microglial cells and changes their transcriptional profile. To verify our hypothesis, we treated primary microglia and BV2 cells with IL-1β. IL-1β treatment resulted in the expression of genes associated with a DAM signature, such as *Apoe*, *Axl*, *Clec7a*, and *Il6*; in comparison, genes associated with a homeostatic microglia signature, such as *Fcrls*, *P2ry12*, *Tgfbr1*, *Teme119*, and *Sall1*, were decreased (Fig. 5B). Elevated expression of APOE coincided with a decrease in P2RY12 and FCRLS expression following IL-1β treatment (Fig. 5C–E, Fig. S3F). Thus, these data suggest that during peripheral infection, GSDMD induces innate immune training and neuroinflammation in the CNS by driving epigenetic and phenotypic changes in microglia, that are dependent on IL-1R.

3.5. CNS immune training induced by pyroptosis of peripheral myeloid cells exacerbates PD pathogenesis

Previous studies have demonstrated that immune training of microglia exacerbates cerebral β-amyloidosis and promotes the pathology of Alzheimer's disease[21]. To explore whether GSDMD-induced innate immune training exacerbates PD-like neuropathology in an IL-1R-dependent way, we utilized the *N*-methyl-4-phenyl-1,2,3,6-tetrahydropyridine (MPTP)-induced experimental model of PD and anti-IL-1β antibody treatment following LPS exposure. The data show that treatment with IL-1β antibody significantly attenuated LPS-induced disease in MPTP-induced PD mouse model compared to WT mice, as indicated by the reduction in microglia activation and decreased loss of dopaminergic neurons. Notably, antibody treatment rescued the disease phenotype in WT mice to comparable levels in *Gsdmd*$^{-/-}$ mice (Supporting Information Fig. S4A). To determine whether GSDMD deficiency in peripheral cells or CNS-resident cells contributes to the suppression of PD-like neuropathology, we treated bone marrow chimeric mice with MPTP and LPS. Co-administration of MPTP with LPS treatment resulted in a significant reduction in microglia activation and loss of dopaminergic neurons in irradiated mice reconstituted with *Gsdmd*$^{-/-}$ or *Nlrp3*$^{-/-}$ bone marrow, compared to WT mice reconstituted with WT bone marrow (Fig. S4B). Thus, inflammasome-induced pyroptosis contributes to the peripheral immune stimuli in an IL-1R-dependent way, which causes alterations in brain immune responses and affects PD pathology.

A30P mice carry a human *SNCA* mutant transgene linked to familial PD, in which α-synuclein deposit develops from 6 months of age and usually develops a progressive phenotype including synucleinopathy, neurodegeneration, loss of striatal dopamine, and locomotor dysfunction. We evaluated the behavior and pathology changes of 9-month-old A30P mice in response to an IP injection of LPS or vehicle control (Supporting Information Fig. S5A). A30P mice administered a single dose of LPS exhibited an increase in PD-related behavioral phenotypes such as the hindlimb clasping test, open field test, climbing test, and rotarod test when compared to control mice (Fig. S5B and S5C). Consistently, we observed no obvious difference in the level of Triton-X (TX)-
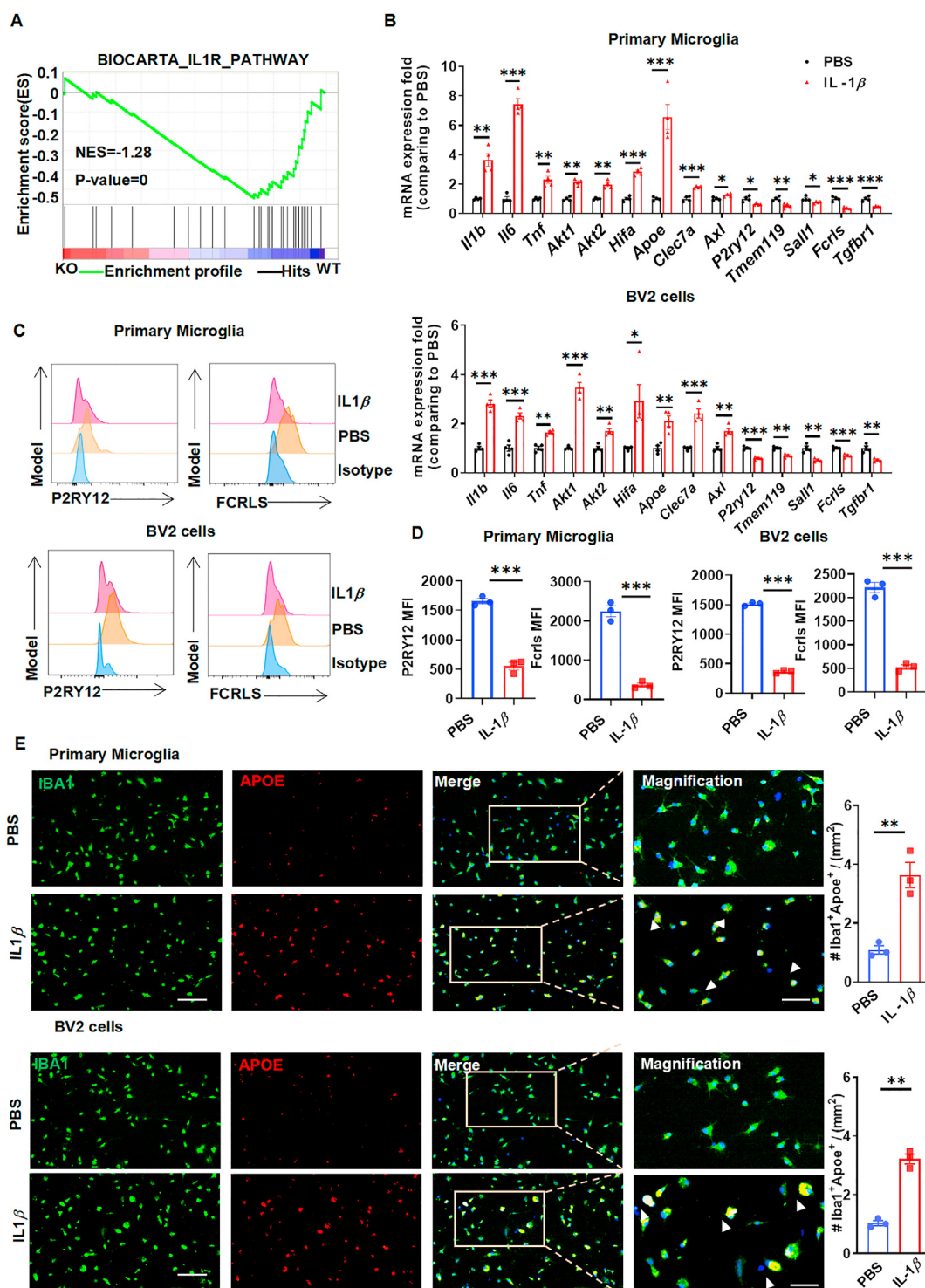
Figure 5 IL-1β signaling promotes the microglial phenotypic switch from homeostasis to disease. (A) GSEA for the genes associated with the "IL-1 receptor signaling pathway" in microglia from RNA-seq data. (B) Quantitative PCR analysis of indicated genes in primary microglia or BV2 cells treated with 20 ng/mL IL-1β for 6 h. (C, D) Flow cytometry (FACS) analysis of P2RY12 and FCRLS expression in primary microglial or BV2 cells treated with 20 ng/mL IL-1β for 24 h. Data are presented as representative plots (C) and summary graphs of quantified mean fluorescence intensity (D). (E) Immunofluorescence analysis of APOE expression in primary microglia (upper) or BV2 cells (lower) treated with 20 ng/mL IL-1β for 24 h. Scale bar, 50 μm. Quantification of IBA1 and APOE puncta colocalization (hollow arrowheads) per 100 × image. Data are pooled from three independent experiments. Data shown are mean ± SEM; *$P < 0.05$, **$P < 0.01$, ***$P < 0.001$ (unpaired t-test).
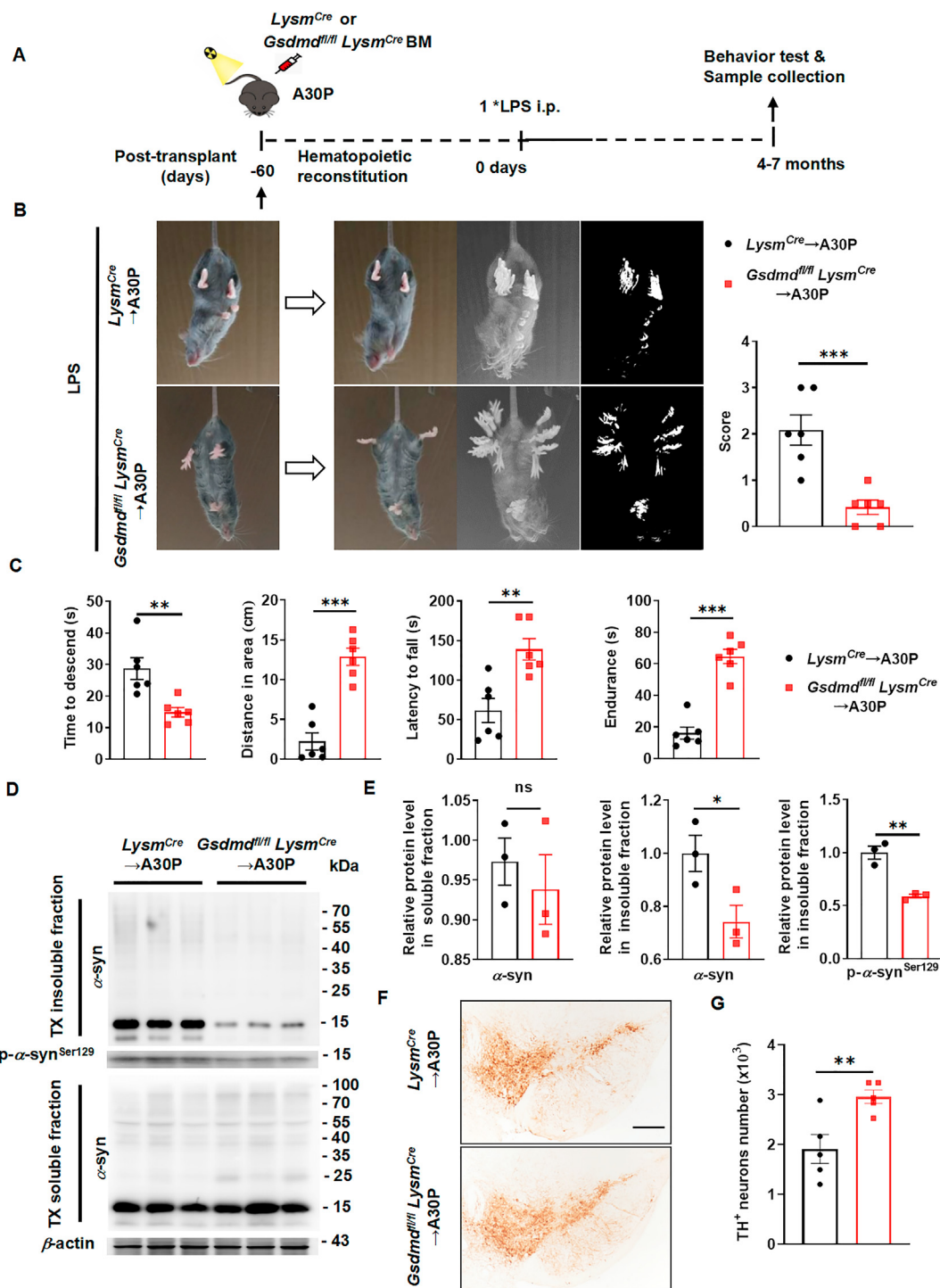
Figure 6 Peripheral myeloid cellular GSDMD-involved innate immune memory exacerbates Parkinson's disease (PD)-like symptoms in A30P mice. (A) Schematic representation of the experiments in (B−G). (B) Hindlimb clasping phenotype of mice in (A). Data are shown as representative pictures and quantified scores ($n = 6$ per group). (C) Behavior test analysis. Open filed test, pole test, and accelerated rotarod test were recorded and analyzed ($n = 6$ per group). (D, E) Immunoblot analysis of insoluble phosphorylated and total α-synuclein aggregates, soluble total α-synuclein in brain SN tissue. Data are shown as representative pictures (D) and quantified relative expression (E) ($n = 3$ per group). (F, G) Immunohistochemistry analysis of dopamine neurons (TH) in brain SN tissue. Scale bar, 200 μm. Data are shown as representative pictures (F) and quantified cell numbers (G) ($n = 5$ per group). Data shown are mean ± SEM; *$P < 0.05$, **$P < 0.01$, ***$P < 0.001$ (unpaired t-test).

soluble α-synuclein, but a significantly increased TX-insoluble total and phosphorylated α-synuclein in LPS treated mice (Fig. S5D and S5E). Consequently, the loss of dopaminergic neurons in the SNc was also increased in mice treated with LPS (Fig. S5F and S5G). Thus, peripheral LPS exposure exacerbates the pathogenesis of PD A30P mice.

Next, we sought to determine if the peripheral NLRP3−GSDMD axis mediates the exacerbation of PD in A30P
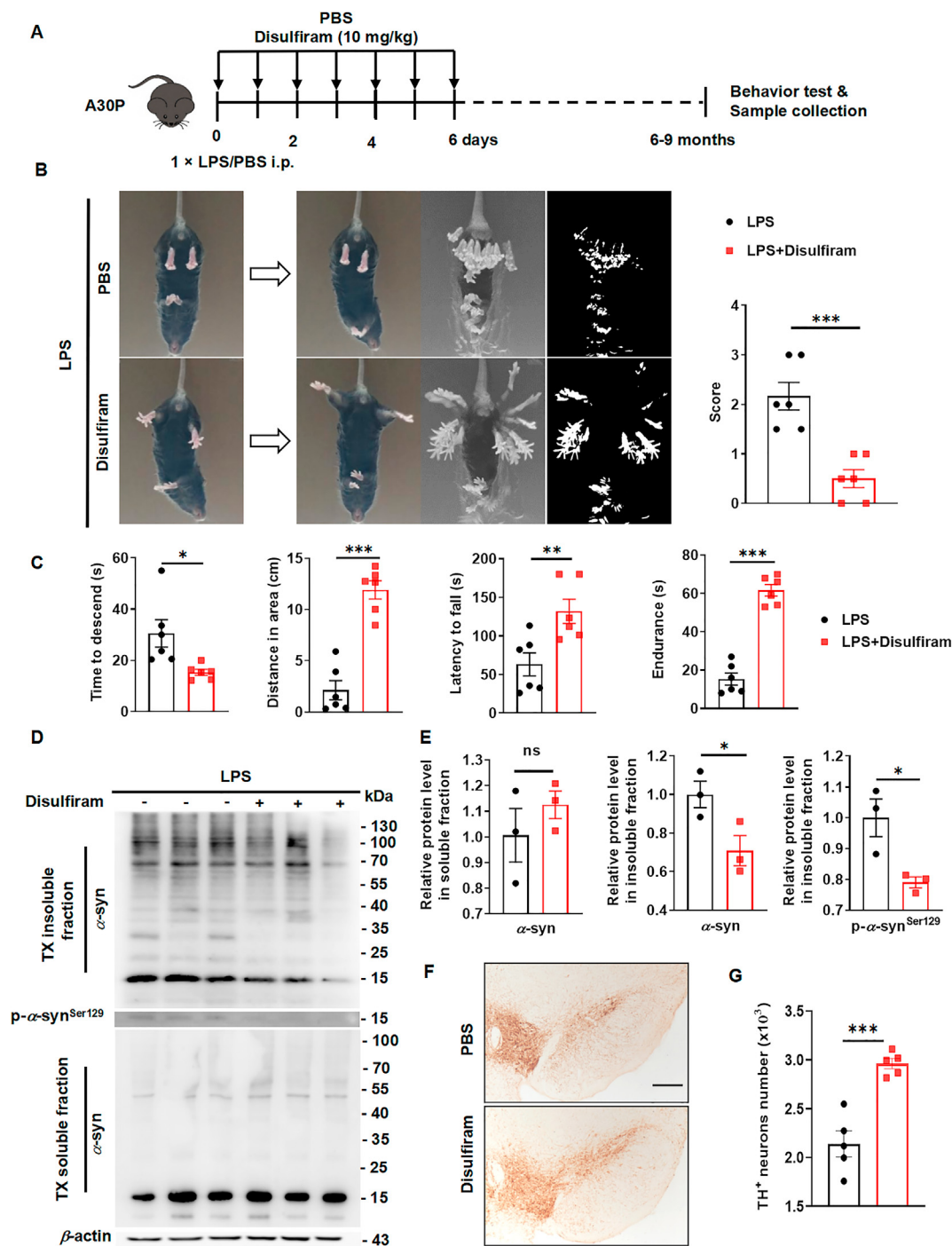
Figure 7 The inhibitory drug targeting GSDMD attenuates PD-like symptoms in LPS-stimulated A30P mice. (A) Schematic representation of the experiments in (B−G). (B) Hindlimb clasping phenotype of mice in (A). Data are shown as representative pictures and quantified scores (*n* = 6 per group). (C) Behavior test analysis. Open filed test, pole test, and accelerated rotarod test were recorded and analyzed (*n* = 6 per group). (D, E) Immunoblot analysis of insoluble phosphorylated and total α-synuclein aggregates, soluble total α-synuclein in brain SN tissue. Data are shown as representative pictures (D) and quantified relative expression (E) (*n* = 3 per group). (F, G) Immunohistochemistry analysis of dopamine neurons (TH) in brain SN tissue. Scale bar 200 μm. Data are shown as representative pictures (F) and quantified cell numbers (G) (*n* = 5 per group). Data shown are mean ± SEM; *$P < 0.05$, **$P < 0.01$, ***$P < 0.001$ (unpaired *t*-test).

mice following LPS exposure. A30P mice were irradiated and reconstituted with bone marrow from *Gsdmd*^{fl/fl}*Lysm*^{Cre}, *Nlrp3*^{fl/fl}*Lysm*^{Cre}, or *Lysm*^{Cre} mice. LPS was administered 2 months post-transfer of bone marrow and evaluated for pathological

phenotypes at 9 months of age (Fig. 6A, Supporting Information Fig. S6A). Mice reconstituted with *Lysm*^{Cre} bone marrow exhibited a significant increase in PD behavioral changes, indicated by results from the hindlimb clasping test, open field test,

climbing test, and rotarod test, compared to mice reconstituted with *Nlrp3*^{fl/fl}*Lysm*^{Cre} or *Gsdmd*^{fl/fl}*Lysm*^{Cre} bone marrow (Fig. 6B and C, Fig. S6B and S6C). In addition, insoluble total and phosphorylated α-synuclein in the midbrain from mice that received *Nlrp3*^{fl/fl}*Lysm*^{Cre} or *Gsdmd*^{fl/fl}*Lysm*^{Cre} bone marrow decreased considerably overmice reconstituted with *Lysm*^{Cre} bone marrow (Fig. 6D and E, Fig. S6D and S6E), and demonstrated a loss of dopaminergic neurons from the SNc (Fig. 6F and G, Fig. S6F and S6G). Thus, these data suggest that blocking innate immune training in the CNS by peripheral NLRP3 and GSDMD deficiency, alleviates augmented LPS-induced PD pathology in A30P mice.

3.6. GSDMD inhibitor attenuates neuropathology in LPS-stimulated A30P mice

Given that immune training induced by peripheral GSDMD promotes neuropathology in A30P mice, we assessed whether pharmacological inhibition of GSDMD would alleviate the PD symptoms. Disulfiram is a GSDMD inhibitor that prevents oligomerization, pore formation, and pyroptotic cell death[41]. Therefore, we administered disulfiram for 7 consecutive days following LPS treatment of A30P mice. Disulfiram treatment impaired LPS-accelerated PD development in the A30P mice as evidenced by a reduction in PD-related behavior phenotypes, decreased insoluble total and phosphorylated α-synuclein, and decreased loss of dopaminergic neurons from the SNc (Fig. 7A−G). Our results show that, in addition to the GSDMD inhibitor disulfiram, the NLRP3 inhibitor MCC950 also exhibited a protective effect on PD in several studies[42,43], which exemplifies the potential value in targeting NLRP3 and GSDMD for PD therapy. However, whether MCC950 can also regulate the training of microglia remains to be seen. Altogether, these results indicate that the blockade of pyroptosis is a therapeutic strategy for PD.

4. Discussion

Classical immunological memory is usually recognized as a secondary immune response to pathogens that have been previously encountered and is dependent on populations of clonally expanded antigen-specific T and B lymphocytes. Conceptually, it has been traditionally appreciated that only adaptive immunity can establish and retain immunological memory. However, recent studies have revealed that innate immune myeloid cells can also exhibit immunological memory[11,44]. Notably, immune training in microglia is essential for neuroinflammation that is triggered in response to peripheral pathogen infection[21], but the precise molecular mechanism by which this process occurs is unknown. In this study, we found that GSDMD-induced pyroptosis is activated in response to a single dose of LPS and is subsequently suppressed when exposed to a second dose of LPS in peripheral myeloid cells. LPS-induced inflammasome activation in peripheral myeloid cells promoted microglial immune training, which exacerbated PD in an IL-1R-dependent manner.

Inflammasome components, such as NLRP3, caspase-1, and GSDMD, are highly expressed in myeloid cells[29]. Consistently, reconstituting irradiated mice with NLRP3 or GSDMD deficient bone marrow found that NLRP3 and GSDMD deficiency in peripheral myeloid cells inhibited neuroinflammation. Recent studies have identified subsets of microglia which are characterized by their specific expression signatures, such as DAM and microglial neurodegenerative phenotype (MGnD)[45−47]. In addition, microglia undergo epigenetic transcriptional reprogramming, which is indispensable for developing immune memory[12,21,48,49]. RNA-seq and ATAC-seq analysis of microglia following the LPS challenge revealed that the most prominent up-regulated responses in microglia without immune training from *Gsdmd*^{−/−} mice were associated with inflammation. Many DAM core genes (*e.g.*, *Apoe*,
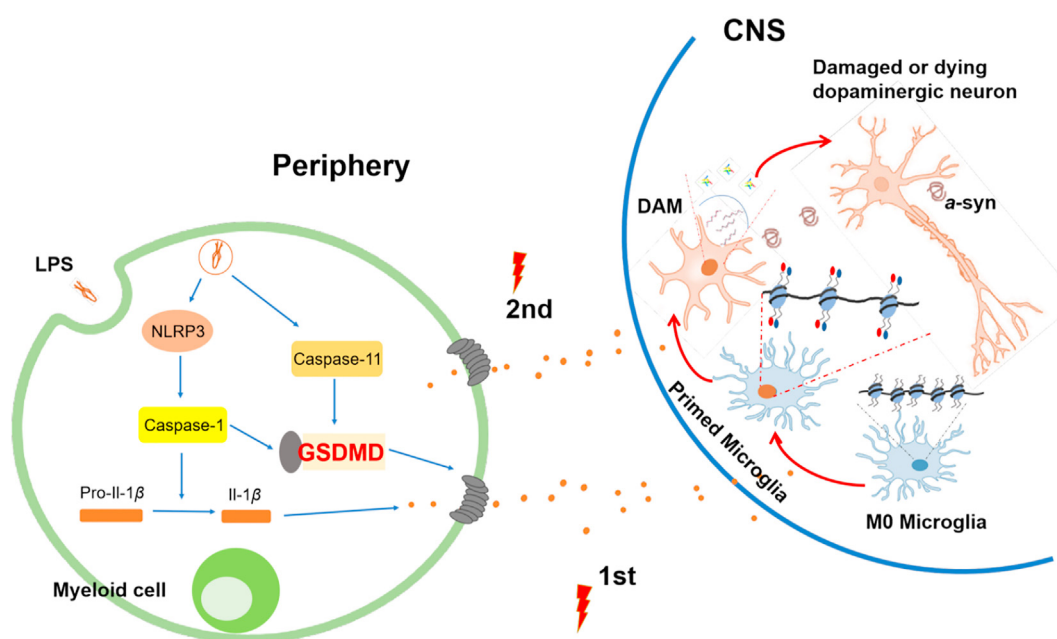

Figure 8   Model for GSDMD in peripheral infection mediated microglial innate immune memory during PD. Briefly, peripheral infection triggers NLRP3 and GSDMD activation to release pro-inflammatory cytokines, such as IL-1β, which promote epigenetic and transcriptional changes in microglia. These changes turn homeostatic microglia into a "primed state", which is more sensitive to secondary stimuli from periphery infection or cerebral α-syn deposition; eventually leading to PD-like symptoms.

Cxcl1, *Il1r2*, *Il12a* and *Il6*) were transcriptionally decreased, and many homeostatic microglial core genes (*e.g.*, *P2ry12*, *Sall1*, *Tgfbr1*, *Fcrls* and *Tmem119*) were transcriptional increased in microglia from *Gsdmd*$^{-/-}$ mice. Moreover, the expression of *Akt1*, *Akt2*, *Hif1a*, *Egln1* and *Egln2* involved in the mTOR and HIF1α pathway was also down-regulated in microglia from *Gsdmd*$^{-/-}$ mice. These genes have been previously linked to innate immune memory[21,37]. Genes associated with the changes in microglial expression signatures occur due to epigenetic changes.

IL-1β has been reported to cross the intact BBB and enter the CNS parenchyma[50]. Consistently, we demonstrated that IL-1β treatment converts microglia from homeostatic microglia (M0) to DAM. Although IL-18, the other major downstream cytokines of inflammasome activation, was significantly increased in serum after LPS treatment, our data showed that only a small fraction of IL-18 entered CNS after one or two doses of LPS. Therefore, we speculate that NLRP3—GSDMD activation in peripheral myeloid cells promotes IL-1β and IL-18 production; however, only IL-1β can enter the CNS parenchyma to stimulate microglial polarization and promote neuroinflammation. The mechanisms which restrict IL-18 entry to the CNS warrant future investigation. Our data also shows peripheral neutralization of IL-1β could protect the dopaminergic neuron loss in the LPS-exacerbated PD mouse model. In addition, a phase 2 clinical trial of canakinumab in mild Alzheimer's disease with peripheral inflammation has been recently initiated. Therefore, neutralizing peripheral IL-1β may be a potential target in PD therapy, and the clinical performance of canakinumab on PD is highly expected. Our work also provides a possible mechanism for this potential therapeutic option.

Although numerous epidemiological studies have verified the association between peripheral infection and PD, the detailed mechanisms of this connection remain largely unknown. To investigate the neuropathology affected by peripheral inflammation, we administered LPS to mimic peripheral bacterial infection in chemically-induced and transgenic experimental models of PD. Remarkably, we identified an intrinsic role of peripheral myeloid cells for NLRP3 and GSDMD in promoting peripheral bacterial infection-induced PD. Viral infections, including influenza virus, herpes simplex virus, hepatitis C virus, and Epstein-Barr virus, are all considered risk factors for the pathogenesis of PD[2,51−53]. However, it is unclear if the NLRP3, GSDMD, or other inflammasomes regulates PD pathogenesis in response to viral infections, which will also be interesting topics to explore.

5. Conclusions

Our study revealed the role that GSDMD-induced pyroptosis plays in initiating microglial innate immune training by peripherally activating myeloid cells. We propose a model in which peripheral myeloid cell-intrinsic GSDMD-induced pyroptosis promotes IL-1β production, crosses the BBB to induce microglial immune training after the first exposure of LPS, and thereby exacerbates PD when encountering second inflammatory stimuli such as MPTP treatment or synuclein A30P overexpression (Fig. 8). Thus, targeting the peripheral pyroptosis may be a potential therapeutic strategy for bacterial infection-related PD.

Author contributions

Conflicts of interest

The authors declare no conflicts of interest.

Appendix A. Supporting information

Supporting data to this article can be found online at https://doi.org/10.1016/j.apsb.2023.04.008.

References

1. Johnson ME, Stecher B, Labrie V, Brundin L, Brundin P. Triggers, facilitators, and aggravators: redefining Parkinson's disease pathogenesis. *Trends Neurosci* 2019;**42**:4−13.

2. Smeyne RJ, Noyce AJ, Byrne M, Savica R, Marras C. Infection and risk of Parkinson's disease. *J Parkinsons Dis* 2021;**11**:31−43.

3. Nielsen HH, Qiu J, Friis S, Wermuth L, Ritz B. Treatment for *Helicobacter pylori* infection and risk of Parkinson's disease in Denmark. *Eur J Neurol* 2012;**19**:864−9.

4. Chiang HL, Lin CH. Altered gut microbiome and intestinal pathology in Parkinson's disease. *J Mov Disord* 2019;**12**:67−83.

5. Dobbs RJ, Dobbs SM, Weller C, Bjarnason IT, Oxlade NL, Charlett A, et al. Role of chronic infection and inflammation in the gastrointestinal tract in the etiology and pathogenesis of idiopathic parkinsonism. Part 1: eradication of *Helicobacter* in the cachexia of idiopathic parkinsonism. *Helicobacter* 2005;**10**:267−75.

6. Kaur T, Uppoor A, Naik D. Parkinson's disease and periodontitis—the missing link? A review. *Gerodontology* 2016;**33**:434−8.

7. Matheoud D, Cannon T, Voisin A, Penttinen AM, Ramet L, Fahmy AM, et al. Intestinal infection triggers Parkinson's disease-like symptoms in *Pink1*$^{-/-}$ mice. *Nature* 2019;**571**:565−9.

8. Muldoon LL, Alvarez JI, Begley DJ, Boado RJ, Del Zoppo GJ, Doolittle ND, et al. Immunologic privilege in the central nervous

system and the blood−brain barrier. *J Cerebr Blood Flow Metabol* 2013;**33**:13−21.

9. Daneman R, Prat A. The blood−brain barrier. *Cold Spring Harbor Perspect Biol* 2015;**7**:a020412.

10. Quintin J, Cheng SC, van der Meer JW, Netea MG. Innate immune memory: towards a better understanding of host defense mechanisms. *Curr Opin Immunol* 2014;**29**:1−7.

11. Netea MG, Joosten LA, Latz E, Mills KH, Natoli G, Stunnenberg HG, et al. Trained immunity: a program of innate immune memory in health and disease. *Science* 2016;**352**:aaf1098.

12. Saeed S, Quintin J, Kerstens HH, Rao NA, Aghajanirefah A, Matarese F, et al. Epigenetic programming of monocyte-to-macrophage differentiation and trained innate immunity. *Science* 2014;**345**:1251086.

13. Biswas SK, Lopez-Collazo E. Endotoxin tolerance: new mechanisms, molecules and clinical significance. *Trends Immunol* 2009;**30**:475−87.

14. Kleinnijenhuis J, Quintin J, Preijers F, Joosten LA, Ifrim DC, Saeed S, et al. Bacille Calmette-Guerin induces NOD2-dependent nonspecific protection from reinfection *via* epigenetic reprogramming of monocytes. *Proc Natl Acad Sci U S A* 2012;**109**:17537−42.

15. Quintin J, Saeed S, Martens JHA, Giamarellos-Bourboulis EJ, Ifrim DC, Logie C, et al. *Candida albicans* infection affords protection against reinfection *via* functional reprogramming of monocytes. *Cell Host Microbe* 2012;**12**:223−32.

16. Christ A, Günther P, Lauterbach MAR, Duewell P, Biswas D, Pelka K, et al. Western diet triggers NLRP3-dependent innate immune reprogramming. *Cell* 2018;**172**:162−175.e14.

17. Gómez-Nicola D, Schetters ST, Perry VH. Differential role of CCR2 in the dynamics of microglia and perivascular macrophages during prion disease. *Glia* 2014;**62**:1041−52.

18. Godbout JP, Chen J, Abraham J, Richwine AF, Berg BM, Kelley KW, et al. Exaggerated neuroinflammation and sickness behavior in aged mice following activation of the peripheral innate immune system. *FASEB J* 2005;**19**:1329−31.

19. Ramaglia V, Hughes TR, Donev RM, Ruseva MM, Wu X, Huitinga I, et al. C3-dependent mechanism of microglial priming relevant to multiple sclerosis. *Proc Natl Acad Sci U S A* 2012;**109**: 965−70.

20. Palin K, Cunningham C, Forse P, Perry VH, Platt N. Systemic inflammation switches the inflammatory cytokine profile in CNS Wallerian degeneration. *Neurobiol Dis* 2008;**30**:19−29.

21. Wendeln AC, Degenhardt K, Kaurani L, Gertig M, Ulas T, Jain G, et al. Innate immune memory in the brain shapes neurological disease hallmarks. *Nature* 2018;**556**:332−8.

22. Paludan SR, Pradeu T, Masters SL, Mogensen TH. Constitutive immune mechanisms: mediators of host defence and immune regulation. *Nat Rev Immunol* 2021;**21**:137−50.

23. Lamkanfi M, Dixit VM. Mechanisms and functions of inflammasomes. *Cell* 2014;**157**:1013−22.

24. Heneka MT, McManus RM, Latz E. Inflammasome signalling in brain function and neurodegenerative disease. *Nat Rev Neurosci* 2018;**19**: 610−21.

25. Shi J, Zhao Y, Wang K, Shi X, Wang Y, Huang H, et al. Cleavage of GSDMD by inflammatory caspases determines pyroptotic cell death. *Nature* 2015;**526**:660−5.

26. Liu X, Zhang Z, Ruan J, Pan Y, Magupalli VG, Wu H, et al. Inflammasome-activated gasdermin D causes pyroptosis by forming membrane pores. *Nature* 2016;**535**:153−8.

27. Storek KM, Monack DM. Bacterial recognition pathways that lead to inflammasome activation. *Immunol Rev* 2015;**265**:112−29.

28. Burdette BE, Esparza AN, Zhu H, Wang S. Gasdermin D in pyroptosis. *Acta Pharm Sin B* 2021;**11**:2768−82.

29. Li S, Wu Y, Yang D, Wu C, Ma C, Liu X, et al. Gasdermin D in peripheral myeloid cells drives neuroinflammation in experimental autoimmune encephalomyelitis. *J Exp Med* 2019;**216**:2562−81.

30. Jackson-Lewis V, Przedborski S. Protocol for the MPTP mouse model of Parkinson's disease. *Nat Protoc* 2007;**2**:141−51.

31. Shang J, Ma S, Zang C, Bao X, Wang Y, Zhang D. Gut microbiota mediates the absorption of FLZ, a new drug for Parkinson's disease treatment. *Acta Pharm Sin B* 2021;**11**:1213−26.

32. Lee E, Hwang I, Park S, Hong S, Hwang B, Cho Y, et al. MPTP-driven NLRP3 inflammasome activation in microglia plays a central role in dopaminergic neurodegeneration. *Cell Death Differ* 2019;**26**:213−28.

33. Liu Z, Yan M, Liang Y, Liu M, Zhang K, Shao D, et al. Nucleoporin Seh1 interacts with Olig2/Brd7 to promote oligodendrocyte differentiation and myelination. *Neuron* 2019;**102**:587−601.e7.

34. Sedelis M, Hofele K, Auburger GW, Morgan S, Huston JP, Schwarting RK. MPTP susceptibility in the mouse: behavioral, neurochemical, and histological analysis of gender and strain differences. *Behav Genet* 2000;**30**:171−82.

35. Liu Y, Liu T, Zhou Y, Li W, Wang M, Song N, et al. Impeding the combination of astrocytic ASCT2 and NLRP3 by talniflumate alleviates neuroinflammation in experimental models of Parkinson's disease. *Acta Pharm Sin B* 2022;**13**:662−77.

36. Chagniel L, Robitaille C, Lacharité-Mueller C, Bureau G, Cyr M. Partial dopamine depletion in MPTP-treated mice differentially altered motor skill learning and action control. *Behav Brain Res* 2012; **228**:9−15.

37. Cheng SC, Quintin J, Cramer RA, Shepardson KM, Saeed S, Kumar V, et al. mTOR- and HIF-1α-mediated aerobic glycolysis as metabolic basis for trained immunity. *Science* 2014;**345**:1250684.

38. Evavold CL, Ruan J, Tan Y, Xia S, Wu H, Kagan JC. The pore-forming protein gasdermin D regulates interleukin-1 secretion from living macrophages. *Immunity* 2018;**48**:35−44.e6.

39. Chang J, Burkett PR, Borges CM, Kuchroo VK, Turka LA, Chang CH. MyD88 is essential to sustain mTOR activation necessary to promote T helper 17 cell proliferation by linking IL-1 and IL-23 signaling. *Proc Natl Acad Sci U S A* 2013;**110**:2270−5.

40. Gulen MF, Kang Z, Bulek K, Youzhong W, Kim TW, Chen Y, et al. The receptor SIGIRR suppresses Th17 cell proliferation *via* inhibition of the interleukin-1 receptor pathway and mTOR kinase activation. *Immunity* 2010;**32**:54−66.

41. Hu JJ, Liu X, Xia S, Zhang Z, Zhang Y, Zhao J, et al. FDA-approved disulfiram inhibits pyroptosis by blocking gasdermin D pore formation. *Nat Immunol* 2020;**21**:736−45.

42. Gordon R, Albornoz EA, Christie DC, Langley MR, Kumar V, Mantovani S, et al. Inflammasome inhibition prevents α-synuclein pathology and dopaminergic neurodegeneration in mice. *Sci Transl Med* 2018;**10**:eaah4066.

43. Huang S, Chen Z, Fan B, Chen Y, Zhou L, Jiang B, et al. A selective NLRP3 inflammasome inhibitor attenuates behavioral deficits and neuroinflammation in a mouse model of Parkinson's disease. *J Neuroimmunol* 2021;**354**:577543.

44. Netea MG, Latz E, Mills KH, O'Neill LA. Innate immune memory: a paradigm shift in understanding host defense. *Nat Immunol* 2015;**16**: 675−9.

45. Deczkowska A, Keren-Shaul H, Weiner A, Colonna M, Schwartz M, Amit I. Disease-associated microglia: a universal immune sensor of neurodegeneration. *Cell* 2018;**173**:1073−81.

46. Song WM, Colonna M. The identity and function of microglia in neurodegeneration. *Nat Immunol* 2018;**19**:1048−58.

47. Krasemann S, Madore C, Cialic R, Baufeld C, Calcagno N, El Fatimy R, et al. The TREM2−APOE pathway drives the transcriptional phenotype of dysfunctional microglia in neurodegenerative diseases. *Immunity* 2017;**47**:566−581.e9.

48. Ostuni R, Piccolo V, Barozzi I, Polletti S, Termanini A, Bonifacio S, et al. Latent enhancers activated by stimulation in differentiated cells. *Cell* 2013;**152**:157−71.

49. Kaikkonen MU, Spann NJ, Heinz S, Romanoski CE, Allison KA, Stender JD, et al. Remodeling of the enhancer landscape during macrophage activation is coupled to enhancer transcription. *Mol Cell* 2013;**51**:310−25.

50. Sadowska GB, Chen X, Zhang J, Lim YP, Cummings EE, Makeyev O, et al. Interleukin-1β transfer across the blood−brain barrier in the ovine fetus. *J Cerebr Blood Flow Metabol* 2015;**35**:1388−95.

51. Camacho-Soto A, Faust I, Racette BA, Clifford DB, Checkoway H, Searles Nielsen S. Herpesvirus infections and risk of Parkinson's disease. *Neurodegener Dis* 2020;**20**:97–103.

52. Wijarnpreecha K, Chesdachai S, Jaruvongvanich V, Ungprasert P. Hepatitis C virus infection and risk of Parkinson's disease: a systematic review and meta-analysis. *Eur J Gastroenterol Hepatol* 2018;**30**:9–13.

53. Hsieh JC, Lue KH, Lee YL. Parkinson-like syndrome as the major presenting symptom of Epstein-Barr virus encephalitis. *Arch Dis Child* 2002;**87**:358.